Appendix A: Supplementary data

Supplementary Figure S1. Global Comparison of (h+k)=even versus (h+k)=odd
An analysis of phase relationships in the projection data of the rectangular crystal forms suggested the presence of c222 symmetry. In this two-sided plane group, reflections for which (h+k)=odd are absent everywhere in the molecular transform. However, due to noise and local breaks of symmetry, these absences are not always strictly observed in the images, which would preclude enforcement of the symmetry and adversely affect calculations of phase origins as well as lattice lines. To independently confirm that the symmetry was present in the 3D data, we analyzed the signal-to-noise ratio distribution in the two populations of reflections. Specifically, (h+k)=even (white bars) and (h+k)=odd (dark bars) were written out into separate data files. The files were then merged using the phase origins that had been calculated for the (h+k)=even set, and the quality of the signal-to-noise ratio (IQ) was tabulated for each of the two data sets by simply counting the IQ1-8 reflections in each data set. The average IQ was 5.7 for (h+k)=even and 7.2 (h+k)=odd. The histograms further illustrated that the vast majority of measurements with high to moderate signal-to-noise ratios were contained in the (h+k)=even half of the data. This was consistent with the presence of c222 symmetry. Moreover, the histogram distribution also justified the removal of the (h+k)=odd reflections, which ultimately have to be eliminated from the data at any rate if c222 symmetry were to be enforced.

Supplementary Figure S2. Phase errors for projection data
The program PLOTALL was used to plot the individual phase error for each structure factor after averaging of data from the various images. Phase errors are encoded as follows: 1, <8°; 2, <14°; 3, <20°; 4, <30°; 5, <40°; 6, <50°; 7, <80°; 8,<90°, where 90° is random; errors larger than 30˚ are indicated by decreasing box sizes. A) Phase error plot for data of unstained stargazin crystals belonging to the less complex of the two c222 forms. Data were averaged in p1, which is the reason why the full half of the transform is shown. While averages were significant to better than 10Å, the projection was only calculated to 15Å because completeness of the data beyond that resolution was low. Phase error plots for the simple (B) and complex (C) c222 forms. D) Phase error plot for the p6 crystal form. B)-D) all plots represent the combined phase error obtained after averaging and rounding to 0/180˚.

Supplementary Figure S3. 6xHis-Stg 2D class averages
Particles were boxed out from seventeen raw micrographs using semi-automated particle picking in EMAN into boxes of 100x100 square pixels (Ludtke et al., 1999). The raw particles were normalized, high- and low-pass filtered, and centered. After discarding bad particles, 2548 particles were subjected to several iterations of reference-free 2D alignment and classification using multivariate statistical analysis and multi-reference alignment in IMAGIC to a final 100 classes (van Heel et al., 1996). The scale bar (lower right-hand corner) equals 100 Å.

Supplementary Figure S4. Select lattice lines at a range of resolutions
Only the phase part of the fit is shown in each case. Lines are plotted at 1/Å along the x-axis. Resolutions are for the respective (h,k,0) projection term. Lattice line (0,16) is

shown to demonstrate that c222 symmetry constraints were obeyed in the 3D-transform.

Supplementary Figure S5. Point spread function plots for determining effective resolution cutoffs

Using a point spread function obtained for a simulated data set with an in-plane resolution cutoff of 16Å as a reference (A), effective resolution cutoffs were determined by comparison as in-plane cutoffs of x = 22.5Å, y = 20.2Å (B) and a vertical cutoff of 31.1Å (C) from the point spread function of the experimental data. Grid spacing corresponds to 10Å. Peaks were contoured at half height (solid line) in line with the Raleigh criterion for resolution.

Supplementary Figure S1

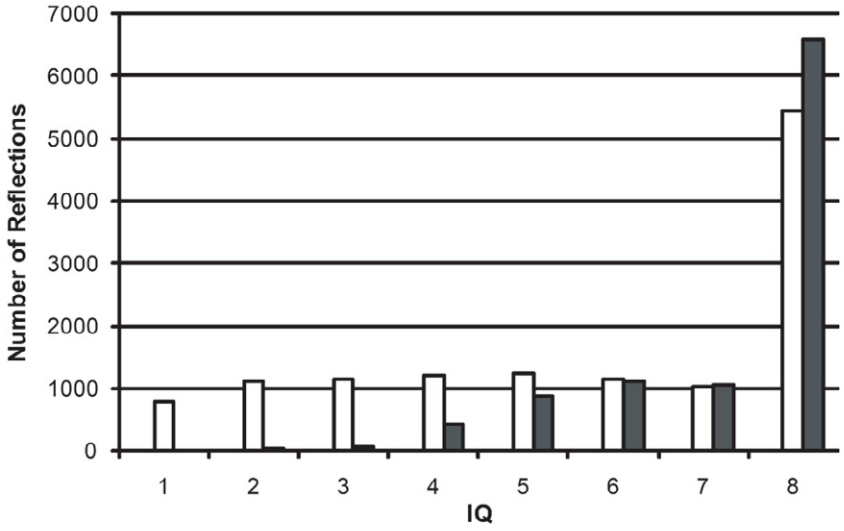

Supplementary Figure S2

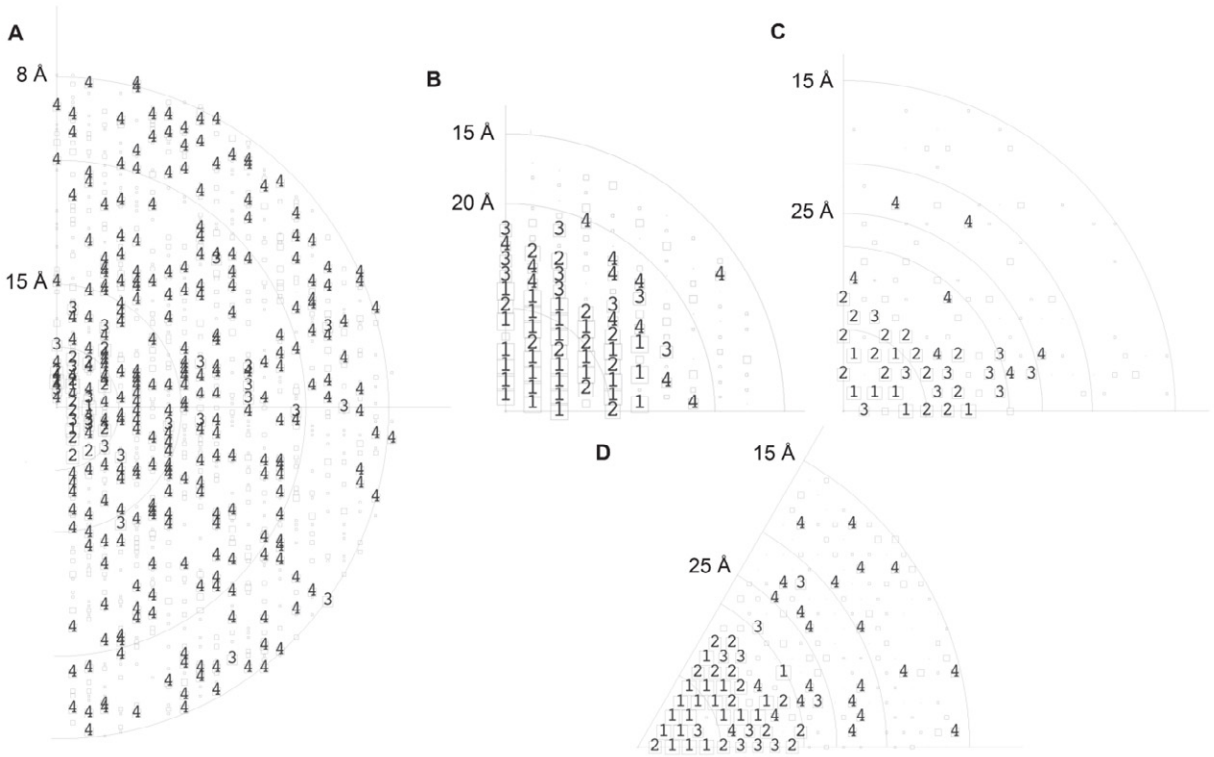

Supplementary Figure S3

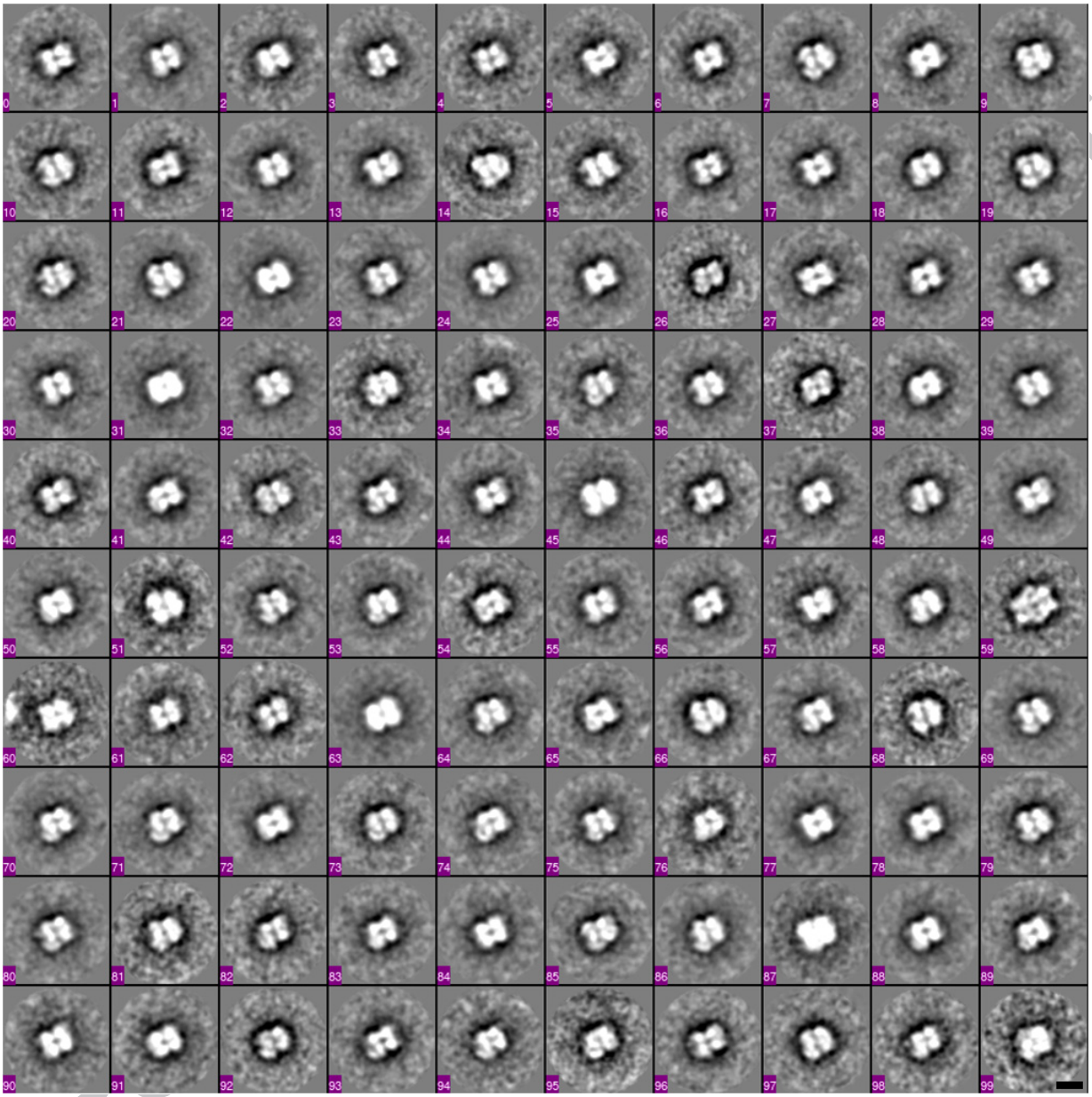

Supplementary Figure S4

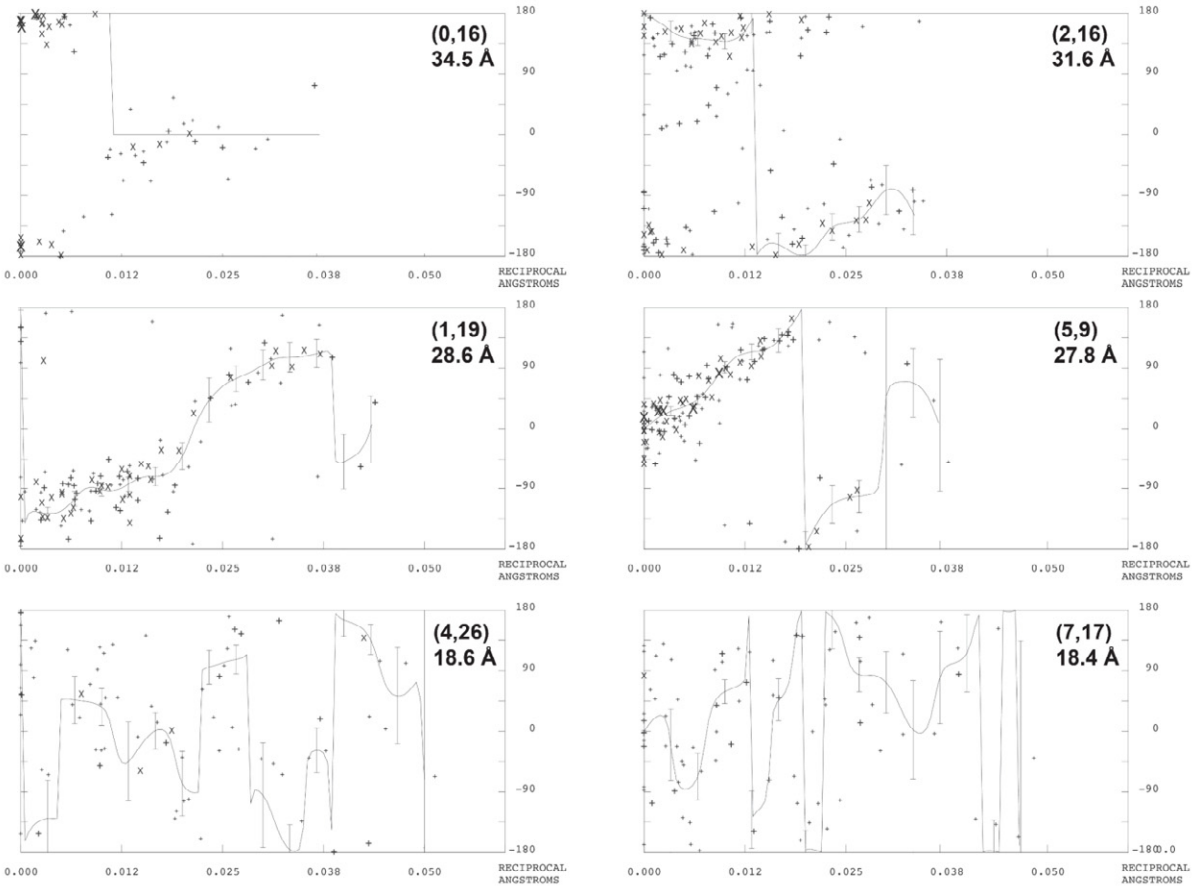

Supplementary Figure S5

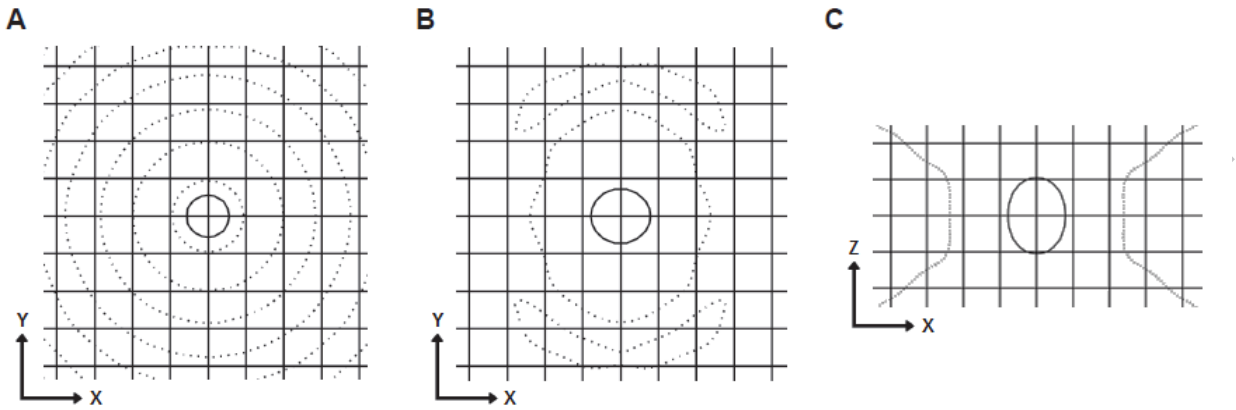

References

S.J. Ludtke, P.R. Baldwin, and W. Chiu, EMAN: semiautomated software for high-resolution single-particle reconstructions, *J. Struct. Biol.* **128** (1999), pp. 82-97.

M. van Heel, G. Harauz, E.V. Orlova, R. Schmidt, and M. Schatz, A new generation of the IMAGIC image processing system, *J. Struct. Biol.* **116** (1996), pp. 17-24.